The interacting Wolf-Rayet galaxy Mkn 8

César Esteban and David I. Méndez

Instituto de Astrofísica de Canarias, E-38200 La Laguna, Tenerife, Canary Islands, Spain (cel,dmendez@ll.iac.es)

Abstract. We present results of narrow-band and broad-band optical CCD imaging together with intermediate-resolution spectroscopy of the Wolf-Rayet galaxy Mkn 8. Analysis of the morphology and kinematics of the object indicates that the strong star formation episode we are witnessing in Mkn 8 is the product of the interaction of two (or three) disk galaxies. The chemical abundances and abundance ratios measured in the brightest knots suggest that the interacting galaxies are chemically evolved gas-rich objects, perhaps late-type spirals.

Key words: stars: Wolf-Rayet – galaxies: individual: Mkn 8 – galaxies: interactions – galaxies: kinematics and dynamics – galaxies: starburst

1. Introduction

The reason why H II galaxies are forming stars at very high rates is still a matter of current debate. A popular hypothesis is that interaction between gas rich galaxies can trigger the bursts. However some large systematic searches for optical bright companions of H II galaxies have failed to detect such companions (Campos-Aguilar & Moles 1991; Campos-Aguilar et al. 1993; Rosenberg et al. 1994; Telles & Terlevich 1995). A possible solution of this problem is the interaction with dwarf H I clouds (Brinks 1990; Taylor et al. 1993, 1995 and 1996; Stil & Israel 1998) or dwarf optical companions (see Esteban & Méndez 1999).

A number of H II galaxies show a broad He II 4686 Å spectral feature, related to the presence of Wolf-Rayet (WR) stars in the ionizing clusters. Because of this, Conti (1991) called them WR galaxies. According to the population synthesis models (e.g. Cerviño & Mas-Hesse 1994; Meynet 1995), the presence of this feature is an indication of the extreme youthfulness of the burst. There is an increasing number of WR galaxies showing evidences of interactions and merging processes as for example: NGC1741 and H31A, (members of the Hickson compact group 31; Rubin, Ford, & Hunter 1990); II Zw 40 (Brinks & Klein 1988); ESO 148-IGO2 (Bergvall & Johansson 1985); ZW0855+06 (Méndez et al. 1999a); Mkn 1094 (Brinks 1990; Walter et al. 1997; Méndez et al. 1999b); and POX 4 and Tol 35 (Méndez & Esteban 1999). In a recent compilation, Esteban &

Méndez (1999) indicate that the interacting and merging nature of the smallest WR galaxies can only be detected when deep, high-resolution images and spectra are available.

Markaryan 8 (Mkn 8) also known as IC 2184, Zw VII 156 or VV 644 is an emission-line or H II galaxy with a peculiar morphology. It was described firstly by Vorontsov-Vel'yaminov (1962) as an interacting pair of coalescent galaxies. Markaryan (1967) describes it as a nest of blue objects, and finally, according to Zwicky (1968) Mkn 8 is a blue posteruptive quartet consisting of two bar-shaped and two spherical compact regions. All these descriptions are based only on the morphology of the galaxy but all agree with the interacting nature of the object. Casini & Heidman (1976) classified it as belonging to the group of clumpy irregular galaxies.

Khachikyan (1974) carried out the first spectroscopical study of Mkn 8. He concludes that the galaxy consists of two main members with a radial velocity difference of about 150–200 km s^{-1}. According to Vorontsov-Vel'yaminov et al. (1981) these two members are merging and divided both in three compact components or superassociations. Kunth & Joubert (1985) obtain low resolution spectra of Mkn 8 and report the presence of the Wolf-Rayet bump at 4686 Å in the integrated spectrum of the northeast zone of the object. These observations lead Mkn 8 to be classified as a WR galaxy in the catalogue of Conti (1991). Surprisingly, there is not mention about the interacting nature of Mkn 8 in this catalogue nor in the most recent one by Schaerer et al. (1999). Assuming a uniform Hubble flow with H$_o$=75 km s^{-1} Mpc^{-1} and given the value of 3520 km s^{-1} for the recession velocity of the object (see Sect. 3.2), Mkn 8 lies at 46.9 Mpc. At this distance, the spatial scale is about 227 pc arcsec^{-1}.

In this paper we present new optical ground-based observations –with better spatial and spectral resolution than before– of Mkn 8, in order to have a better insight into the interacting nature of this object and of the WR galaxies in general.

2. Observations and data reduction

2.1. Optical imaging

These observations were carried out on 1997 February 4 and 6 at the 2.56-m Nordic Optical Telescope (NOT) at the Roque de los Muchachos Observatory at La Palma (Canary Islands, Spain). We obtained Hα and adjacent continuum together with Johnson

Table 1. Summary of observations.

Observations	Telescope	Date	P.A. (°)	Exposure Time (s)	Spatial Sampling ($''$ pix^{-1})	Spectral Resolution (Å pix^{-1})	$\Delta\lambda$ (Å)	λ_C Filter (Å)
Narrow-band	NOT	97/02/04	....	3×900	0.176	...	...	6640 (Hα)
Imaging	NOT	97/02/04	....	3×600	0.176	...	...	6563 (cont.)
Broad-band	NOT	97/02/06	....	3×400	0.176	...	...	U
Imaging	NOT	97/02/06	....	3×300	0.176	...	...	B
	NOT	97/02/06	....	3×300	0.176	...	...	V
Intermediate	3.5mCAHA	99/01/26	21	4×900	0.56	1.08	3500–5500	...
Dispersion	3.5mCAHA	99/01/26	21	4×900	0.56	0.55	5900–7000	...
Spectroscopy	3.5mCAHA	99/01/26	73	4×900	0.56	1.08	3500–5500	...
	3.5mCAHA	99/01/26	73	4×900	0.56	0.55	5900–7000	...
	3.5mCAHA	99/01/26	4	3×1200	0.56	1.08	3500–5500	...
	3.5mCAHA	99/01/26	4	3×1200	0.56	0.55	5900–7000	...

U, B, and V high-resolution CCD images using the StanCam Camera with a TEK CCD detector (1024×1024 pixels) with a pixel size of 24 μm^2 and a spatial resolution of 0.176$''$ pixel^{-1}. The narrow band filters for the Hα and red-continuum images (centered at 6640 and 6563 Å respectively and with a FWHM of 50 Å in both cases) were selected taking into account the recession velocity of the object (Khachikyan 1974; Kunth & Joubert 1985). Three exposures of each filter were added to obtain a good signal-to-noise and an appropriate removal of cosmic rays in the final images. The images were bias subtracted, flat-fielded and flux calibrated following standard procedures.

For the narrow-band filters, the absolute flux calibration was achieved taking short exposures of the calibration stars BD+75°325 and HZ 44 from the catalogue of Oke (1990). The absolute flux calibration of all the broad-band images was performed taking short exposures of the stars 96 21 and 104 490 from the catalogue of Landolt (1992).

The images were sky subtracted and corrected for atmospheric and interstellar extinction using our spectroscopic data. All the reduction process was done with the IRAF[1] package. The mean seeing during the observations was about 1$''$. The log of all the observations can be found in Table 1.

2.2. Intermediate resolution spectroscopy

Observations were carried out on 1999 January 26 with the TWIN spectrograph at the Cassegrain focus of the 3.5m telescope of the Centro Astronómico Hispano-Alemán (CAHA) at Calar Alto (Almería, Spain). Two CCD SITe with a configuration of 800×1024 pixels of 15 μm each were used in the blue and red arms of the spectrograph. The slit was 240$''$ long and 1.2$''$ wide. Two gratings were used, the T06 of 1200 lines mm^{-1} in the red arm and the T08 of 600 lines mm^{-1} in the blue arm. These gratings give reciprocal dispersions of 36 and 72 Å mm^{-1}, respectively. The blue spectra cover from 3500

to 5500 Å and the red ones from 5770 to 6850 Å. The spatial resolution is 0.56$''$ pixel^{-1} in both cases.

Three slit positions of Mkn 8 were observed at different angles. Three or four exposures were taken in each case. The different position angles were chosen in order to cover the most interesting zones taking into account the morphology of the galaxy. Comparison lamp exposures of He-Ar were taken after each set of object spectra. The correction for atmospheric extinction was performed using an average curve for the continuous atmospheric extinction at Calar Alto Observatory. The absolute flux calibration was performed from the observation of the standard star Feige 66 (Massey et al. 1988). All the CCD frames were reduced using the standard IRAF LONGSLIT reduction package.

3. Results

3.1. Optical imaging

In Fig. 1 we show the B image, $U - B$, and $B - V$ maps, the continuum-subtracted Hα image (at high and low intensities), and the Hα equivalent width, W(Hα), map of Mkn 8. The morphology of the object is rather similar in all the filters and consists of an irregular (almost triangular) ring of bright knots or condensations immersed in a diffuse envelope. Rests of a satellite track are visible in the B image and the color maps.

The eastern branch of the galaxy consists of three knots (#5, #9, and #12) on an almost straight line of about 30$''$ long. The brightest knot of the galaxy in all the filters is the northern edge of this branch (knot # 5). The western branch consists of two main bright knots (#7 and #11) and a number of other fainter ones (#6, #10, #13, #16, #17, and #18) forming an arc with its concave side towards the eastern branch. Knot #7 is somewhat elongated along the direction to the bright knot #5, both branches almost coalesce in this zone. It is interesting the presence of two concentric short arc-shaped structures extending off to the side of the brightest knot #5. These structures were firstly reported by Vorontsov-Vel'yaminov et al. (1981) and interpreted as a product of interaction. In our images, these features are visible

---

[1] IRAF is distributed by NOAO which is operated by AURA, Inc., under cooperative agreement with NSF
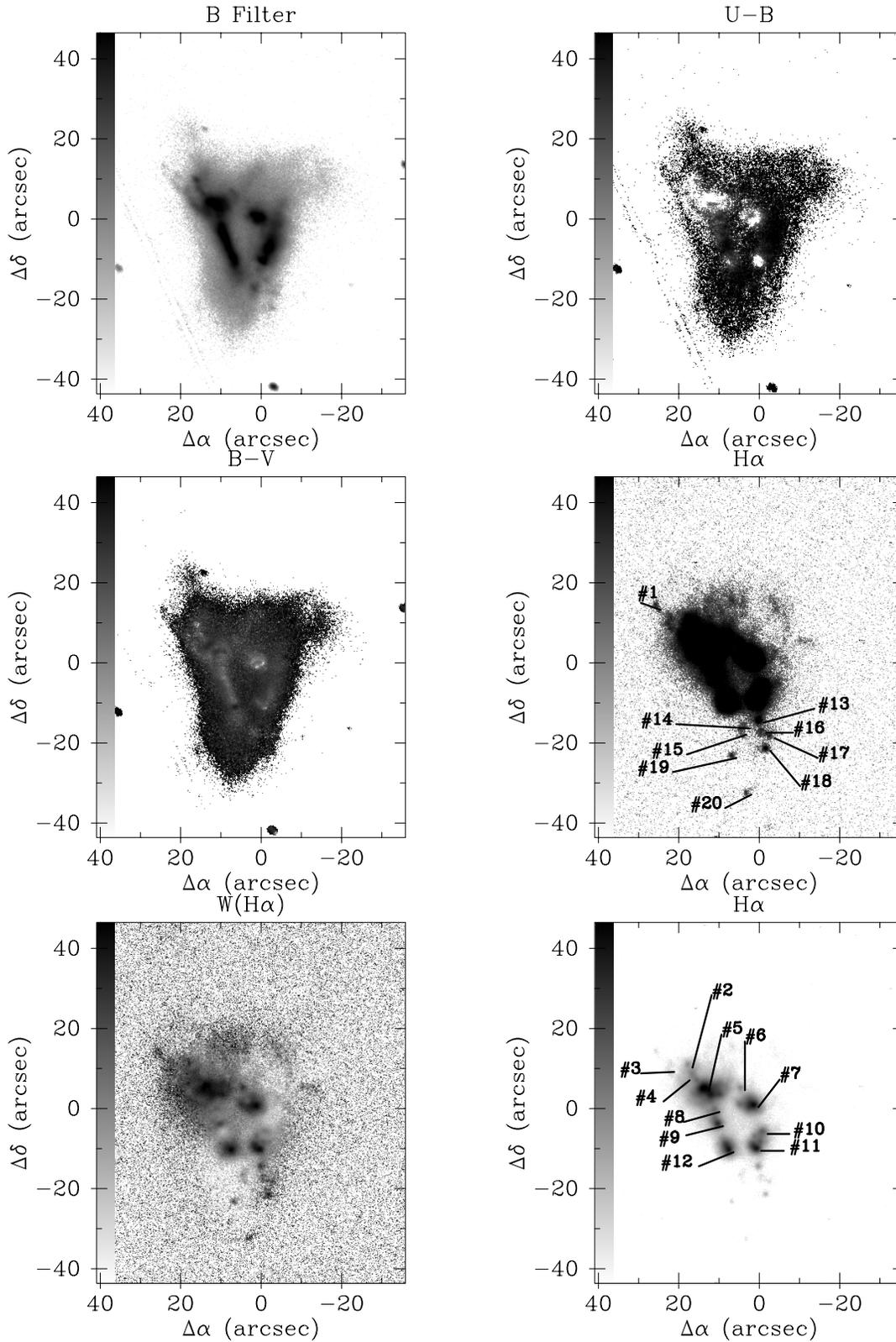
Fig. 1. Logarithmic gray-scale representation of the B image (upper left), $U - B$ color map (upper right), $B - V$ color map (middle left), continuum subtracted Hα image at low-intensity levels (middle right), Hα equivalent width map (W(Hα), lower left), and continuum subtracted Hα image at high-intensity levels (lower right). The gray-scale ranges (form white to black) are: B from 23.36 to 18.80 mag arcsec^{-2}, $U - B$ from -0.9 to -0.3 mag arcsec^{-2}, $B - V$ from -0.2 to 0.8 mag arcsec^{-2}, Hα at low-intensity from 1.17×10^{-16} to 1.17×10^{-15} erg cm^{-2} s^{-1} arcsec^{-2}, W(Hα) from 0 to 579 Å, Hα at high-intensity from 2.93×10^{-16} to 4.68×10^{-14} erg cm^{-2} s^{-1} arcsec^{-2}. The different star-forming knots analysed are indicated in both Hα images. North is at the top and east is to the left.

Table 2. Results of aperture photometry.

Knot	$\log(L(H\alpha))$ (cgs)	M_B (mag)	$U-B$ (mag)	$B-V$ (mag)	$-W(H\alpha)$ (Å)
#1	38.01	-10.11 ± 0.10	-1.61 ± 0.24	0.59 ± 0.17	2415 ± 1035
#2	38.84	-13.01 ± 0.03	-0.96 ± 0.07	0.12 ± 0.05	180 ± 10
#3	38.37	-11.62 ± 0.05	-1.04 ± 0.13	0.32 ± 0.09	395 ± 50
#4	38.79	-12.56 ± 0.03	-0.96 ± 0.09	0.16 ± 0.06	255 ± 15
#5	41.16	-18.18 ± 0.01	-0.87 ± 0.01	0.15 ± 0.01	335 ± 5
#6	39.15	-13.63 ± 0.02	-0.80 ± 0.06	0.19 ± 0.04	170 ± 5
#7	40.69	-17.63 ± 0.01	-0.81 ± 0.01	0.02 ± 0.01	170 ± 5
#8	39.23	-14.68 ± 0.01	-0.69 ± 0.04	0.04 ± 0.02	83 ± 5
#9	40.10	-16.87 ± 0.01	-0.59 ± 0.01	0.03 ± 0.01	87 ± 5
#10	39.40	-15.23 ± 0.01	-0.47 ± 0.03	0.18 ± 0.02	55 ± 5
#11	40.32	-16.78 ± 0.01	-0.81 ± 0.01	0.11 ± 0.01	144 ± 5
#12	40.63	-17.52 ± 0.01	-0.62 ± 0.01	0.15 ± 0.01	145 ± 5
#13	39.07	-13.61 ± 0.01	-0.67 ± 0.03	0.34 ± 0.03	105 ± 5
#14	37.75	-11.77 ± 0.04	-0.55 ± 0.15	0.25 ± 0.08	30 ± 5
#15	38.01	-12.04 ± 0.04	-0.53 ± 0.13	0.26 ± 0.07	45 ± 5
#16	38.46	-12.48 ± 0.03	-0.81 ± 0.10	0.26 ± 0.06	105 ± 10
#17	38.37	-11.98 ± 0.04	-0.67 ± 0.13	0.33 ± 0.07	190 ± 20
#18	38.76	-12.52 ± 0.03	-0.95 ± 0.09	0.41 ± 0.06	385 ± 30
#19	38.30	-12.11 ± 0.04	-0.60 ± 0.13	0.42 ± 0.07	90 ± 5
#20	38.02	-9.54 ± 0.13	-2.29 ± 0.26	1.21 ± 0.20	...
Total	41.63	-20.36 ± 0.01	-0.58 ± 0.01	0.34 ± 0.01	95 ± 5

in the Hα and broad-band images and, therefore, they should be of stellar nature. In Fig. 2 we show the low-intensity structures visible in our V image (which have been reported previously by Homeier & Gallagher 1999). It is remarkable the presence of a large-scale arc or loop of stellar nature surrounding the northeast part of the galaxy which seems to be aligned with the aforementioned smaller but brighter concentric arcs. There is also a fainter extension towards the southeast of the galaxy which extends further away the field of our image. This feature seems to be aligned with the southern part of the western branch of the galaxy and seems to originate from this zone.

On the other hand, there are also some diffuse filaments in the Hα image at the northwest of the galaxy. This part of the galaxy is also extended in the broad-band images and presents also an arc-shaped feature at the edge but not coincident with the Hα filaments. The Hα filamentary structures could be related to the mechanical action of the massive stars as it has been observed in other WR galaxies as He 2–10 (Méndez et al. 1999c) and similar objects (Marlowe et al. 1995, Martin 1998).

We detect 20 different individual star-forming knots in the continuum-subtracted Hα image using the IRAF FOCAS package at our resolution limit of about 227 pc at the distance of Mkn 8. FOCAS looks for local maxima and minima in the number counts of each pixel in the image, detecting and isolating the different knots. We adopted the criterion that the number counts of each of the pixels of the knot is higher than 3σ (the statistical standard deviation of the image background). All these knots are labelled in Fig. 1. The Hα luminosity, $L(H\alpha)$, $W(H\alpha)$, the absolute blue magnitude, and the $U-B$ and $B-V$ colors of these knots are presented in Table 2. The $L(H\alpha)$ and $W(H\alpha)$
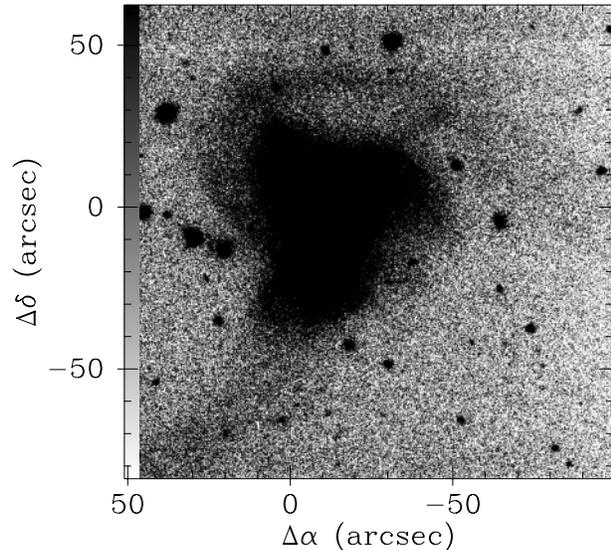
Fig. 2. Low-intensity levels of the V image of Mkn 8. North is at the top and east is to the left.

values have been corrected for [N II] emission. In particular, we have applied the [N II]/Hα ratio measured in each knot for those observed with our intermediate resolution spectroscopy (knots #5, #7, #8, #9, #11,#12). We have assumed an average value of the [N II]/Hα ratio for the rest. The Poissonian uncertainties associated to each quantity are included in Table 2, in the case of $L(H\alpha)$ these uncertainties are always less than 5%. The integrated $U-B$ and $B-V$ colors of the galaxy are slightly bluer (about 0.10 mag in both cases) than those given by Börngen &

Kalloglyan (1975), based on photographic data. The brightest knot, # 5, has an equivalent circular diameter of about 1600 pc, more than 4 times larger than 30 Doradus. The rest of the knots have diameter in the range of about 227 pc (the resolution limit, # 1, # 4, and # 20) to 1400 pc (knot #7). Knot # 5 accounts for the 32% of the integrated Hα flux of the galaxy. In the case of the U, B, and V filters, knot #5 contributes with the 17%, 13% and 11%, respectively of the total emission of the galaxy.

The Hα image and equivalent width map shows that the emission concentrates at the centre of the star-forming knots, with dimensions of the order of the resolution limit. This imposes spatial restrictions on the extension of the star clusters to be of the order or smaller than the seeing disk. On the other hand, the W(Hα) shows variations from knot to knot. If we concentrate on the brightest knots of the galaxy (#5, #7, #9, #11, and #12), we see that #5 shows the largest equivalent width (−335 Å); #7, #11 (both located in the western branch), and #12 present relatively lower values than #5 but higher than #9. The $U − B$ color is qualitatively consistent with the behaviour of W(Hα), in the sense that lower $U − B$ values are correlated with larger equivalent widths.

Using Kennicutt (1988) and the value of the total integrated Hα luminosity (4.5×10^{41} erg s^{-1}) we can derive a number of 1.6×10^6 M$_\odot$ for the mass of the ionizing stars (10–100 M$_\odot$) in the whole galaxy. Assuming an average electron density and temperature of about 100 cm^{-3} and 10000 K, respectively, we obtain a total Q(H^o)=5 × 10^{53} photons s^{-1} and $M_{\rm H\,II} = 1.6 \times 10^7$ M$_\odot$ for the whole galaxy. This value of the total ionizing flux implies the presence of about 8900 O5V stars (assuming a value of Q(H^o) = 5×10^{49} photons s^{-1} per star). In the case of knot #5, the brightest of the galaxy, the number of O5V contained in this knot is about 2900.

Following the population synthesis models for instantaneous bursts of Leitherer & Heckman (1995) and taking into account the value of the W(Hα) of the different knots, it is possible to estimate their age. Assuming a Salpeter inital mass function (IMF)[2] with an upper cut-off of 100 $M_\odot$ and a metallicity of 0.4 $Z_\odot$ (see Sect. 3.2). We estimate that knots #5 and #7 have ages of 4.7 and 5.5 Myr, respectively, and #9, #11, and #12 between 5.8 to 6.6 Myr. The rest of the knots, which are much fainter, have ages between 4.5 Myr (knot #3, very faint, located at the northeast of #5) and 7.8 Myr.

The observed $U − B$ and $B − V$ colors and the models of Leitherer & Heckman (1995) can also be used to obtain an additional estimate of the age of the bursts. In particular, we find that the age obtained from the $U − B$ color is, in all the cases, between 1 and 2 Myr lower than the ages obtained via W(Hα) apart from some low surface brightness knots (#14, #15, and #16), where the differences are large. The age discrepancy in the bright knots could be attributed to several reasons as, for example, absorption of the nebular Hα flux by the spectral features of the underlying stellar population, or contamination of line emission in the B filter. On the other hand, the ages derived making use of the $B − V$ color for the central knots

---

[2] The results are very similar for a Scalo IMF.
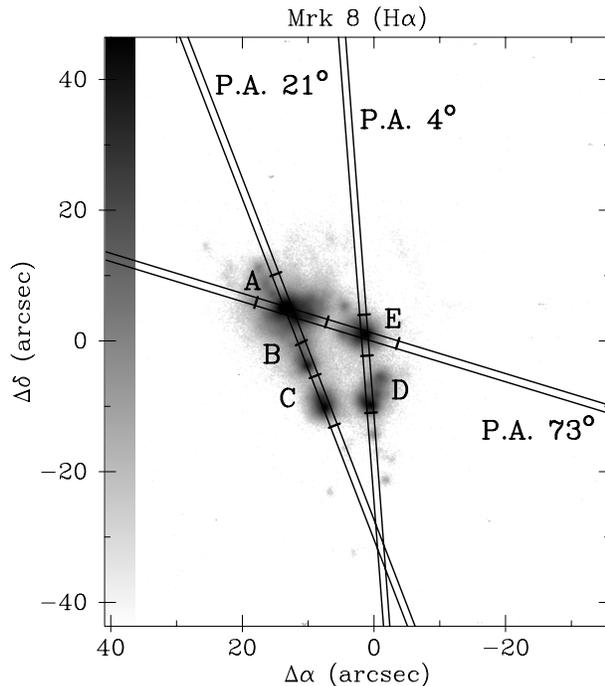
Fig. 3. Slit positions for intermediate-resolution spectroscopy. The gray-scale representation is the continuum-subtracted Hα image of Mkn 8. North is at the top and east is to the left.

(#7, #8, #9, #10, #11, and #12) are broadly consistent with the values obtained with the other two indicators. However, for the other knots the age obtained from $B − V$ is much more larger. This fact could be due to the larger relative contribution of an older underlying population in these zones.

Following the model of Gallagher et al. (1984), and taking into account the value of the total Hα ionizing photons and the integrated blue luminosity of the galaxy, it is possible to derive the current ($\leq 10^7$ yr) star formation rate (SFR) and that related to the past few billion years, which turn out to be 6.40 and 0.48 M$_\odot$ y^{-1} respectively.

3.2. Intermediate resolution spectra

Fig. 3 shows the three slit positions observed for Mkn 8. The different position angles (P.A.s) observed and regions extracted (also shown in the figure) were chosen in order to study the kinematics, physical conditions and chemical abundances of the brightest knots of the galaxy.

In Fig. 4 we present the two-dimensional Hα spectrum for the three P.A.s observed. The vertical bars show the different regions of the spectrum that have been extracted for analysis of their physical conditions and chemical abundances. Each zone has been labeled with a letter from A to E and correspond to one or several of the knots indicated in Figs. 1 and 3 (A to #5; B to #8 and #9; C to #12; D to #11; E to #7).

We have studied the kinematics of the ionized gas via the analysis of the Hα emission line profile along each slit position. We have extracted zones of five pixels wide (2.8″ long) covering
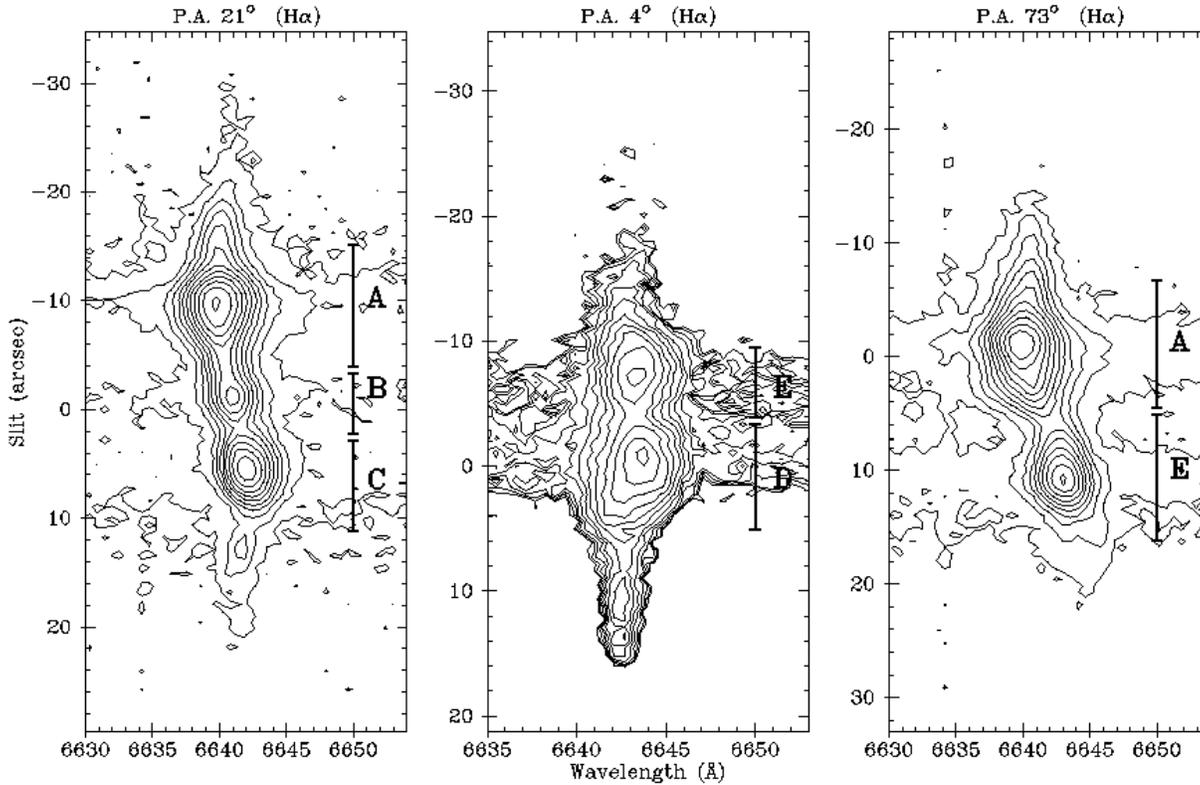
Fig. 4. Contour plots of the two-dimensional Hα profile of Mkn 8 for the three slit positions observed. The different regions selected along the slits for the chemical abundance analysis are indicated and labelled. The top of the plots correspond to the northeast in all cases.
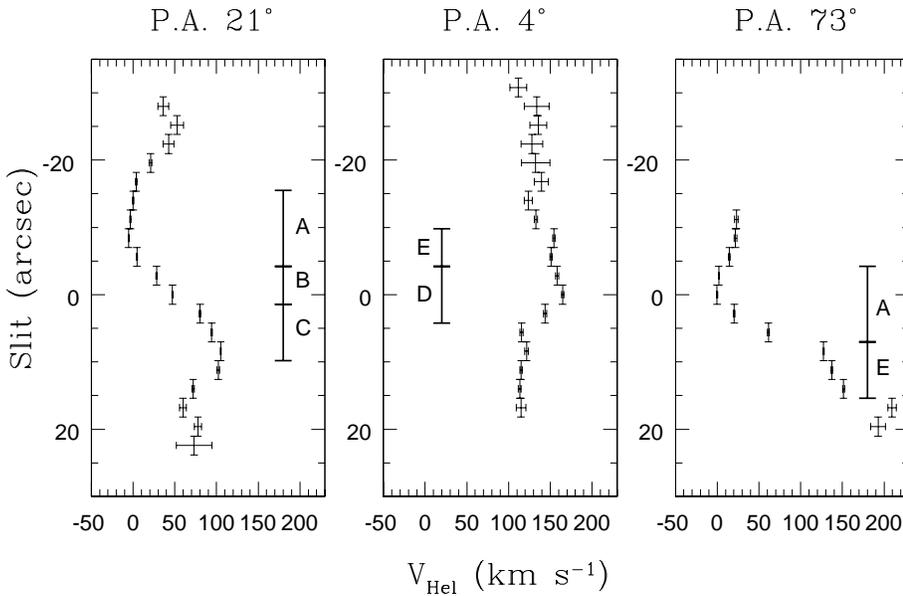
Fig. 5. Position-velocity diagrams for the three slit positions observed for Mkn 8 (obtained from the centroid of the Gaussian fitting of the Hα line profile). The horizontal bars represent the uncertainty of the Gaussian fitting for each point. The different regions selected along the slits for the chemical abundance analysis are indicated and labelled. The top of the plots correspond to the northeast in all cases.

all the extension of the emitting zone in the three slit positions. This analysis has been performed via Gaussian fitting making use of the Starlink DIPSO software (Howarth & Murray 1990). For each single or multiple Gaussian fit, DIPSO gives the fit parameters (radial velocity centroid, Gaussian sigma, FWHM, etc.) and their associated statistical errors. In all the cases, the Hα line emission was well fitted by a single Gaussian fit and

therefore no complex profiles were needed. In Fig. 5 we show the position-velocity diagrams for the three slit positions observed for Mkn 8. All the velocities are referred to the mean heliocentric velocity of knot A (#5) which is 3520 km s^{-1}.

The position-velocity diagrams shown in Fig. 5 are rather complex. The P.A. 21° shows a double-sinusoidal variation in radial velocity with a maximum difference of about 110 km s^{-1}.

The central parts show a smoothly increasing gradient of radial velocity from northeast to southwest and correspond to the three bright knots conforming the eastern branch of the galaxy. This fact suggests that the eastern bar can be interpreted as a rotating solid-body. On the other hand, the slit position at P.A. 4° shows a more constant velocity distribution. However, knots D and E show radial velocities between 20 and 50 km s^{-1} redshifted with respect to the surrounding extended halo of ionized gas. This external halo does not show velocity gradients either to the north or south of the central chain of bright knots. It is difficult to explain the behaviour of the position-velocity diagram of this slit position; it could be produced either by tidal effects or the mechanical action of the massive young population on the gas distribution. In the case of the third slit position, P.A. 73°, the position-velocity diagram of the brightest parts shows also a continuously increasing gradient of radial velocities from the east (knot A) to the west (knot E), with a maximum difference of about 210 km s^{-1} (this large velocity difference between both knots was firstly reported by Khachikyan 1974).

If the central part of the position-velocity diagram of P.A. 21° is interpreted as a solid-body rotation, then we can estimate the Keplerian mass of the eastern branch of the galaxy. Taking into account the half of the maximum velocity difference and the spatial separation corresponding to these maxima, we obtain a mass of $1.3 \times 10^9 \, M_\odot$ for an inclination of 90°. In this case, the northeast half would be the aproaching part of the branch. On the other hand, the position-velocity diagram of P.A. 73° could be also interpreted as a rotation curve, although the gradient is not so smooth and the velocity difference is a factor 2 larger. In this case, the corresponding Keplerian mass is about $4.8 \times 10^9 \, M_\odot$.

As we have commented above, several regions (designated from A to E) were selected to carry out an analysis of their physical conditions and chemical abundances. Line intensities of each spectrum were measured by integrating all the flux in the line between two given limits and over a fitted local continuum. The measurements were made with the SPLOT rutine of the IRAF package. In Fig. 6 we show the spectrum of region A extracted from P.A. 21°.

In order to obtain accurate values of the fluxes of the nebular Balmer lines we have to correct for the underlying stellar absorption. In the case of Mkn 8, absorption wings are evident in the Balmer lines shortward Hβ in all the extracted regions except region A, where the absorption is marginal. We applied a double profile fitting procedure to correct the line fluxes for underlying absorption using the SPLOT rutine. We have assumed a Gaussian profile in emission and a broader Lorentzian one for the absorption component. All the parameters of both components (central wavelength, flux, and width) were kept free in the fitting procedure. The equivalent widths in absorption for Hβ and Hγ are between 6.5 to 9.5 Å. The effect of the correction for absorption on the flux of the emission component is never larger than 5%.

The spectra were corrected for reddening using the Whitford (1958) law and the value of C(Hβ) derived from the ratio between the absorption-corrected Hβ and observed Hα line in-
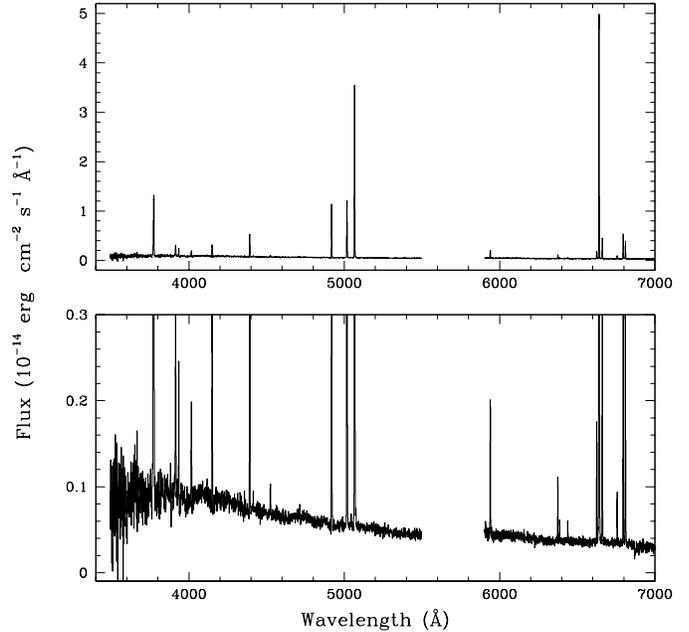
Fig. 6. Intermediate resolution spectrum of region A extracted from P.A. 21°.

tensities as compared with the theoretical values expected for case B recombination using Brocklehurst (1971). The reddening function, $f(\lambda)$, the reddening-corrected line intensity ratios, the reddening coefficient, C(Hβ), the Hβ line flux, F(Hβ), and the equivalent width of several lines, W(Hβ), W(Hα), and W([O III]), are given in Table 3. We estimate that the line intensities are generally accurate within 5% for lines with $I(\lambda)/I$(Hβ) > 1, 10% for lines $I(\lambda)/I$(Hβ) $\sim$ 0.1 and 20% for lines with $I(\lambda)/I$(Hβ) $\sim$ 0.01. The spectra given for regions A and E in Table 3 are the average of two spectra of the same zones obtained from different slit positions (P.A. 21° and P.A. 73° for region A, and P.A. 73° and P.A. 4° for region E, see Fig. 3). The W(Hα) obtained for the same zones of the galaxy from both, the Hα image and the spectra, are consistent (differences smaller than 25%) except in the case of region D, where the discrepancy is a factor three. By definition, equivalent widths are indeed very sensitive to the amount of underlying stellar continuum, an hence to the aperture. Therefore, this large disagreement can be due to the different size and geometry of the apertures taken in both bidimensional photometry and spectroscopy, being much concentrated to the nucleus of #11 in the first case (an almost circular aperture of about 3″ of diameter in the photometry and 8″ × 1.2″ in the spectroscopic observations). We have made an additional estimation of the ages of the bursts using W(Hβ) and models by Leitherer & Heckman (1995), and the results are qualitatively consistent with the ages obtained with W(Hα). The youngest knot is #5 (region A) with an age of about 4 Myr. Knots #7, #9 and #12 have ages of 5.0, 6.6, and 6.0 Myr, respectively.

The spectrum of region A shows a faint broad emission feature around 4650 - 4686 Å, this is produced by the emission of the WR stars (the so-called "WR bump", see Fig. 7). The nebular
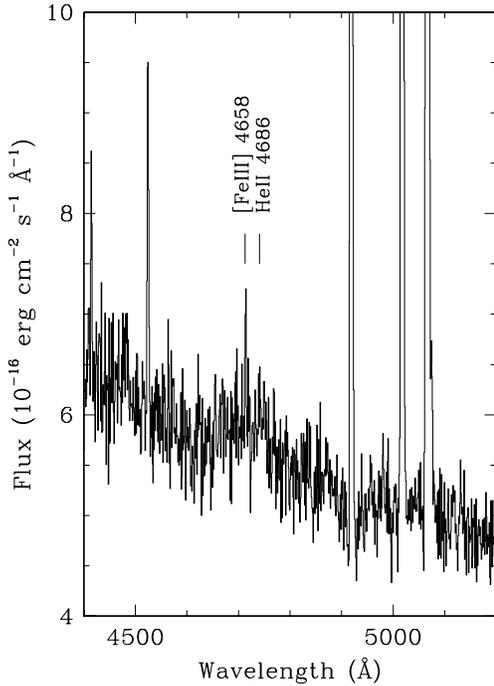
Fig. 7. Section of the spectrum of region A of Mkn 8 showing the zone of the "WR bump". The position of the nebular [Fe III] 4658 Å and He II 4686 Å lines is indicated.

[Fe III] 4658 Å line is relatively very bright and its contribution can be removed easily from the total flux of the bump. Due to its faintness, we can only obtain a highly uncertain measurement of the derredened flux of the broad emission feature, which is about 5×10^{-15} erg cm^{-2} s^{-1} and an equivalent width of about 10.5 Å in emission. These values are roughly similar to the numbers obtained previously by Kunth & Joubert (1985), who measured a flux of 2.5×10^{-15} erg cm^{-2} s^{-1} and an equivalent width of 7.6 Å in emission. Taking into account a distance of 46.9 Mpc for Mkn 8, we obtain a luminosity for the bump of about 2.7×10^{39} erg s^{-1}. The presence of WC stars generates also the bump around 4650 Å but another broad emission feature around 5808 Å produced mainly by the blend of C IV 5801,12 Å lines. Unfortunately, this feature is just at the edge of the red spectra and therefore it is not possible to detect unambiguously its emission. Without this information we cannot determine the relative contribution of each spectral subtype (WN or WC) to the total WR population. Smith (1991) gives that a single WNL star contribute with 3.2×10^{36} erg s^{-1} to the luminosity of the WR bump, whereas a single WC contributes with 5×10^{36} erg s^{-1}. Taking into account these numbers, we obtain a range of $550 - 850$ for the number of WR stars in region A.

Assuming that the spectrum of region A contains the emission of all the WR stars present in knot #5, we can make a rough estimate of the WR/O ratio for this knot. From the Hβ flux given in Table 3 for region A, we derive a number of 1020 O5V stars. This number has to be corrected for the contribution of the WR stars to the ionizing flux (considering 1.7×10^{49} photons s^{-1} per star, Vacca & Conti 1992). Finally, we obtain a number of about 800 O5V stars, which gives a WR/O between 0.7 to 1,

Table 3. Dereddened line intensity ratios.

Line	f(λ)	A	B	C	D	E
3729 [O II]	0.26	230	273	211	269	281
3835 H9	0.24	4	...	...	...	...
3869 [Ne III]	0.23	24	...	24	...	13
3889 He I+H8	0.22	15	...	13	...	9
3969 [Ne III]+H7	0.21	15	...	12	...	9
4101 Hδ	0.18	21	...	11	...	14
4340 Hγ	0.135	45	36	38	32	38
4363 [O III]	0.13	2	...	...	...	...
4471 He I	0.10	4	...	4	...	...
4658 [Fe III]	0.05	1	...	...	...	...
4861 Hβ	0.0	100	100	100	100	100
4959 [O III]	-0.02	109	65	114	51	54
5007 [O III]	-0.03	327	196	326	146	175
5876 He I	-0.23	12	11	11	11	11
6300 [O I]	-0.30	4	9	6	11	7
6312 [S III]	-0.30	1	2	2	...	...
6364 [O I]	-0.31	1	3	2	4	4
6548 [N II]	-0.34	7	14	10	21	15
6563 Hα	-0.34	286	286	286	286	286
6584 [N II]	-0.34	23	45	29	70	50
6678 He I	-0.35	3	3	3	...	3
6717 [S II]	-0.36	28	53	37	68	51
6731 [S II]	-0.36	19	39	27	49	38
F(Hβ)[1]		7.60	1.83	3.36	1.33	3.10
C(Hβ)		0.31	0.28	0.41	0.54	0.46
$-W$(Hβ) (Å)		82	15	26	9	35
$-W$(Hα) (Å)		413	83	166	46	194
$-W$([O III]) (Å)		289	33	92	13	63

[1] in units of 10^{-14} erg cm^{-2} s^{-1}.

an extremely large value. On the other hand, if we consider the Hα luminosity obtained from the bidimensional photometry of knot #5 (this aperture has a size of 41 arcsec^2, a factor three larger than the zone where the spectra of region A have been extracted), we derive a number of 2900 O5V stars (2600 to 2700 after correction for the ionization of the WR stars), which gives a WR/O between 0.20 to 0.33. This ratio is still very large but of the order of other determinations for similar galaxies (see Vacca & Conti 1992).

At this point it would be interesting to discuss about the non-detection of WR features in the star-forming knots of Mkn 8 except in region A (knot #5). At the metallicity of the galaxy ($\sim$ 0.4 Z$_\odot$), population synthesis models of Leitherer & Heckman (1995) for instantaneous burst predict a large population of WR stars for an age between $\sim$ 3 to 6 Myr, and a very sharp decrease after that period. Region A (knot #5) is the youngest burst in the galaxy, having an age of 4.7 Myr from W(Hα) [and 4.0 Myr from W(Hβ)]. The rest of the knots have ages of about 1 Myr or more older. Although the age could be playing an important role in this sense, the different luminosity of each knot can be also a strong reason for the non-detection of the WR feature. For example, region E (knot #7) the brightest knot after region A, has a luminosity almost 3 times lower. Even in the presence of the same WR/O ratio in that knot, the detection of the "WR

Table 4. Physical conditions and chemical abundances

	A	B	C	D	E
N_e([S II]) (cm^{-3})	<100	<100	<100	<100	110
T_e([O III]) (K)	10300	...	...	...	...
R_{23}	6.66	5.34	6.51	4.66	5.10
$T_e(R_{23})$ (K)	9200	8500	9200	8000	8600
12+log O$^+$/H$^+$	7.89	8.34	8.06	8.47	8.34
12+log O^{++}/H$^+$	8.03	8.19	8.19	8.08	8.04
12+log O/H	8.26	...	...	...	...
12+log O/H (R_{23})	8.44	8.54	8.44	8.62	8.51
log N$^+$/O$^+$	−1.26	−1.19	−1.20	−1.05	−1.16
12+log N/H	7.00	7.35	7.24	7.57	7.35
log Ne^{++}/O^{++}	−0.75	...	−0.70	...	−0.68
12+log S$^+$/H$^+$	5.97	6.62	6.36	6.80	6.58
12+log S^{++}/H$^+$	6.35	6.95	6.79	...	...
12+log S/H	6.50	7.12	6.93	>6.80	>6.58
log S/O	−1.76	−1.42	−1.51	> −1.82	> −1.93
He$^+$/H$^+$ (4471)	0.082	...	0.081	...	...
He$^+$/H$^+$ (5876)	0.088	0.078	0.080	0.077	0.078
He$^+$/H$^+$ (6678)	0.080	0.070	0.071	...	0.070
<He$^+$/H$^+$>	0.085	0.076	0.079	0.077	0.076

bump" would be extremely difficult with the signal-to-noise of our spectra (see Figs. 6 and 7).

In Table 4 we show the physical conditions and chemical abundances derived for the five regions selected in the galaxy. The electron density, N_e has been derived from the ratio of the [S II] 6717,31 Å doublet and the five-level program for the analysis of emission-line nebulae of Shaw & Dufour (1995). Electron densities are always near or below the low-density limit ($\leq$ 100 cm^{-3}). A direct determination of the electron temperature, T_e, is only possible for region A. The auroral [O III] 4364 Å line is detected only in this region. For all the regions we have obtained an indirect determination making use of the R_{23} ratio defined as $R_{23} = ([O\,II]\,3726\,Å + [O\,III]\,4959, 5007\,Å)/H\beta$ (the so-called *empirical method*, firstly defined by Pagel et al. 1979) and the calibration by Edmunds & Pagel (1984). The [N II] 5484 Å/[O II] 3726 Å ratios observed in all the regions indicate that the high abundances branch of the diagrams of Edmunds & Pagel (1984) is the appropriate for the galaxy. In the case of region A, the direct and indirect determinations of T_e differs by 1100 K, which is reasonably within the expected uncertainties of the method. The ionic abundances of O$^+$, O^{++}, N$^+$, Ne^{++}, S$^+$, and S^{++} have been derived using the five-level program of Shaw & Dufour (1995), the direct determination of T_e in the case of region A, and the indirect determination of T_e (the only available) for the other regions. The He$^+$/H$^+$ ratio has been derived for the different He I lines observed in each region and using the predicted line emissivities calculated by Smits (1996). We have corrected all the He$^+$/H$^+$ ratios for collisional contribution following the calculations by Kingdon & Ferland (1995).

The total abundances have been determined for O, N, and S and are also included in Table 4. For O, we have considered the standard assumption that the only relevant ionization stages of

O are O$^+$ and O^{++} (we do not see a measurable contribution of nebular He II lines that would suggests the presence of significant O^{3+}). Therefore, O/H = O$^+$/H$^+$ + O^{++}/H$^+$. For N, we have assumed the standard ionization correction scheme based on the similarity between the ionization potential of N$^+$ and O$^+$ (Peimbert & Costero 1969), which is a reasonably good aproximation for an object with the excitation degree of Mkn 8 (see Stasińska 1980). We have measured two ionization stages of S in three of the regions, giving S$^+$/S^{++} from 0.37 to 0.47. With such low S$^+$/S^{++} ratios we do not expect a significant contribution of S^{3+} (see Stasińska 1980). In Table 4 we include the O/H ratio obtained for region A using both the direct and indirect determination of T_e, the difference is about 0.18 dex, being higher in the second case. The O/H abundance in all the regions is relatively high and fairly similar taking into account the large uncertainties of the *empirical method* (about 0.30 dex). Other abundance ratios, comparatively much less dependent on T_e, as N$^+$/O$^+$ and Ne^{++}/O^{++}, also indicate the similar and relatively high chemical content of the different regions.

4. The interacting nature of Mkn 8

Since the pionering works of Toomre (1970) and Toomre & Toomre (1972), it is well known that gravitational interactions between disk galaxies could generate tidal features. In this sense, the presence of the two possible tidal tails we see in Fig. 2 indicates clearly the interacting nature of Mkn 8, and that the interacting galaxies (at least two of them) had rotating disks before their encounter. Its complex dynamical structure, revealed by the position-velocity diagrams shown in Fig. 5, also points out in the same direction. It is striking that the position-velocity diagram of P.A. 21° resembles closely the one obtained by Dufour et al. (1996) for I Zw 18, but the amplitude of radial velocity is much smaller for this last object. Dufour et al. (1996) discover a physically connected low surface brightness companion close to the main body of I Zw 18. It is possible that the gravitational interaction between both companions could be producing the distortion of the velocity field. As in the case of Mkn 8, the brightest central part of I Zw 18 has a smoothly increasing gradient, fact that suggests that it is in simple solid-body rotation. Another similar object is Mkn 297. As Mkn 8, it has been also classified as a clumpy irregular galaxy by Casini & Heidmann (1976). Burenkov (1988) obtained position-velocity diagrams at different P.A.s for Mkn 297, finding a very similar double-sinusoidal behaviour in his spectrum of P.A. 4°. In this sense, it is very significant that Mkn 297 has been also interpreted as an interacting pair of galaxies by many authors (e.g. Vorontsov-Vel'yaminov & Arkhipova 1964; Duflot et al. 1976; Alloin & Duflot 1979). Moreover, numerical N-body simulations made by Taniguchi & Noguchi (1991), have shown that co-planar radial penetration collision between two disk galaxies explains overall morphological properties of Mkn 297. In this sense, we propose that the double-sinusoidal variation in radial velocity shown by the spectrum of P.A. 21° of Mkn 8, could be the effect of the tidal braking of the external parts of a rotating disk. The central recession velocity of the rotating structure is similar to

that of the external gas at the north and south edges, which is about 3580 km s^{-1}.

The morphology of the possible tidal tails shown in Fig. 2 seems also consistent with the picture outlined above. The easten part of the galaxy has an "S" shape, which is specially obvious in the northern part. This reversal of the spatial distribution of the stars can be related with the behaviour of the radial velocity field in that part of the eastern branch of Mkn 8. The gas and stars in the northern outskirts are left behind (reaching more positive velocities) due to the gravitational braking of the rotating disk.

In the case of the western branch, its nature is not so clear. The position-velocity diagram of P.A. 4° does not show clear signs of rotation. This could mean either this branch is not rotating at all or that the plane of rotation of this object is almost perpendicular to our line-of-sight. The average recession velocity of the ionized gas in this slit position is about 3670 km s^{-1}, somewhat larger than the recession velocity of the eastern branch. The morphological and kinematical differences suggest that both, the eastern and western branches might correspond to different galaxies. In the B image shown in Fig. 1, we can see that knots #10 and #11 have faint extensions to the northwest and southwest. These extensions delineate a bar in the spatial distribution of the stars which forms an almost perfect "V" with the eastern branch. In this context, the position of knot #7 is somewhat puzzling, because it appears almost dettached of this bar. This fact does not have a simple explanation. It can be interpreted either by the interaction of two different objects in the western branch (this would imply that we have a triple interacting system) or a strong distortion of the morphology of the galaxy that forms the western branch. On the other hand, the morphology of the southern tail suggests that it is more likely aligned with the western branch.

Another unsolved question is the behaviour of the position-velocity diagram of the P.A. 73°. In principle it resembles a typical solid-body rotation curve, as the change in velocity is much more abrupt than in the case of P.A. 21°. However, it is not possible to distinguish this possibility from the simple overlapping of two knots of emission with relatively different radial velocities.

Unfortunately, the kinematical and morphological analysis of the data obtained does not provide an unambiguous explanation of the true nature of Mkn 8. However, it seems reasonable to propose that Mkn 8 should be the product of the interaction of two or three galaxies. The presence of the two tidal tails indicates that –at least– two of those galaxies should have disks.

Considering the large uncertainties of the indirect estimations of electron temperature, the O/H ratios obtained for the brightests knots do not show significant differences. Moreover, the N$^+$/O$^+$ ratios, weakly dependent of the assumed T_e, are almost coincident. Therefore, the chemical evolution of the interacting galaxies should have been very similar. On the other hand, the relative large metallicity of Mkn 8 indicates –undoubtedly– that it is not a young object, and that other star formation events should have occurred in the past.

The O/H ratios found for Mkn 8 go from 12 + log O/H = 8.26 to 8.61 (from 8.44 to 8.61 including only those values deter-

mined with the *empirical method*). These abundances are of the order or somewhat larger than the oxygen abundances measured for irregular galaxies of the Local Group (with a maximum of 8.34 for the Large Magellanic Cloud, Skillman et al. 1989). In contrast these values are of the order of the O/H ratios obtained for late-type spiral galaxies of the same M_B (see Zaritsky et al. 1994). On the other hand, the integrated blue magnitude of Mkn 8 (-20.36 mag) is larger than those of the brightest irregular galaxies of the Local Group (see Skillman et al. 1989), even if we consider that Mkn 8 consists of two (or even three) interacting objects. The log N$^+$/O$^+$ ratios of the different knots of Mkn 8 (between -1.05 and -1.26) are somewhat lower than the values found for H II regions of the outer Milky Way, which cluster around -1.0 (Vílchez & Esteban 1996), but clearly larger than the typical abundance ratios of irregular galaxies (log N/O about -1.46, Garnett 1990). Therefore, the analysis of the chemical abundances points out that Mkn 8 should be the product of gas-rich chemically evolved objects, perhaps late-type spirals.

5. Conclusions

We have obtained and analyzed detailed optical broad and narrow band imaging together with intermediate resolution spectroscopy of the WR galaxy Mkn 8. Our main results can be summarized as follows:

– The WR galaxy Mkn 8 is now undergoing a strong burst of star formation distributed in a ring of several knots inmersed in a diffuse envelope. These knots are about 4–6 Myr old, as reflected by their W(Hα), W(Hβ), and $U - B$ color.

– We have obtained a rough estimation of the number of WR stars in the northeast knot of Mkn 8 (knot #5 or region A), which is between 550 and 850. This translates into a WR/O ratio of the order of 0.20–0.33 or even larger, in that knot. We do not detect the presence of the "WR bump" at 4650-86 Å in other zones of the galaxy.

– The deep V image shows low-intensity structures of stellar nature that can be interpreted as tidal tails. This fact demonstrates the interacting nature of the object and that at least two of the colliding galaxies have (or had) disks.

– The position-velocity diagrams obtained for the three slit positions observed show complex behaviour, probably due to the interaction process. In the case of P.A. 21°, the position-velocity diagram can be interpreted as a combination of a solid-body rotation and tidal braking of the external parts.

– The chemical abundances –specially the N$^+$/O$^+$ ratio– are relatively high and similar in the brightest knots. This fact indicates that the interacting galaxies are gas-rich chemically evolved objects, perhaps late-type spirals.

In summary, all the observational evidences indicate that the strong star formation episode we are witnessing in Mkn 8 is the product of an interaction process between two (or three) gas-rich, but chemically evolved, disk galaxies. This result highlights the concept that galaxy interactions could be an important channel to produce the strong star formation activity that leads to WR galaxies.

References

Alloin D., Duflot R., 1979, A&A 78, L5

Bergvall N., Johansson L., 1985, A&A 149, 475

Börngen F., Kalloglyan A.T., 1975, Astrophysics 10, 97

Brinks E., 1990, In: Wielen R. (ed.) Dynamics & Interactions of Galaxies. Springer, Berlin, p. 146

Brinks E., Klein U., 1988, MNRAS 231, 63p

Brocklehurst M., 1971, MNRAS 153, 471

Burenkov A.N., 1988, Astrophysics, 28, 26

Campos-Aguilar A., Moles M., 1991, A&A 241, 358

Campos-Aguilar A., Moles M. Masegosa J., 1993, AJ 106, 1784

Casini C., Heidmann J., 1976, A&A 47, 371

Cerviño M., Mas-Hesse J.M., 1994, A&A 284, 749

Conti P.S., 1991, ApJ 377, 115

Conti P.S., Vacca W.D., 1992, ApJ 423, L97

Duflot R., Lombard J., Perrin Y., 1976, A&A 48, 437

Dufour R.J., Esteban C., Castañeda H.O., 1996, ApJ 471, L87

Edmunds M.G., Pagel B.E.J., 1984, MNRAS 211, 507

Esteban C., Méndez D.I., 1999, In: van der Hucht K.A., Eenens P.R.J., Koeningsberger G. (eds.) IAU Symp. 193, Wolf-Rayet Phenomena in Massive Stars and Starburst Galaxies. in press

Gallagher J.S., Hunter D.A., Tutukov A.V., 1984, ApJ 284, 544

Garnett D.R., 1990, ApJ 363, 142

Homeier N.L., Gallagher J.S., 1999, In: van der Hucht K.A., Eenens P.R.J., Koeningsberger G. (eds.) IAU Symp. 193, Wolf-Rayet Phenomena in Massive Stars and Starburst Galaxies. in press

Howarth I.D., Murray J., 1990, SERC Starlink User Note No. 50

Kennicutt R.C., 1988, ApJ 334, 144

Khachikyan E.E., 1974, Astrophysics 8, 311

Kingdon J., Ferland G.J., 1995, ApJ 442, 714

Kunth D., Joubert M., 1985, A&A 142, 411

Landolt A.U., 1992, AJ 104, 340

Leitherer C., Heckman T.M., 1995, ApJS 96, 9

Markaryan B.E., 1967, Astrofizika 3, 55

Marlowe A.T., Heckman T.M., Wyse R.F.G., Schommer R., 1995, ApJ 438, 563

Martin C.L., 1998, ApJ 506, 222

Massey P., Strobel K., Barnes J.V., Anderson E., 1988, ApJ 328, 315

Méndez D.I., Cairós L.M., Esteban C., Vílchez J.M., 1999b, AJ 117, 1688

Méndez D.I., Esteban C., 1999, AJ, in press

Méndez D.I., Esteban C., Balcells M., 1999a, AJ 117, 1229

Méndez D.I., Esteban C., Filipović M.D., et al., 1999c, A&A, in press

Meynet G., 1995, A&A 298, 767

Oke J.B., 1990, AJ 99, 1621

Pagel B.E.J., Edmunds M.G., Blackwell D.E., Chun M.S., Smith G., 1979, MNRAS 189, 95

Peimbert, M., Costero R., 1969, Bol. Obs. Tonantzintla Tacubaya 5, 3

Rosenberg J.L., Salzer J.J., Moody J.W., 1994, AJ 108, 1557

Rubin V.C., Ford W.K., Hunter D.A., 1990, ApJ 365, 86

Schaerer D., Contini T., Pindao M., 1999, A&AS 136, 35

Skillman E.D., Kennicutt R.C. Jr., Hodge P.W., 1989, ApJ 347, 875

Shaw R.A., Dufour R.J., 1995, PASP 107 896

Smith L.F., 1991, In: van der Hucht K.A., Hidayat B. (eds.) IAU Symp. 143, Wolf-Rayet Stars and Interrelations with Other Massive Stars in Galaxies. Dordrecht, Kluwer, 601

Smits D.D., 1996, MNRAS 278, 683

Stasińska G., 1980, A&AS 83, 501

Stil J.M., Israel F.P., 1998, A&A 337, 64

Taniguchi Y., Noguchi M., 1991, AJ 101, 1601

Taylor C., Brinks E., Skilman E.D., 1993, AJ 105, 128

Taylor C., Brinks E., Grashuis R.M., Skilmann E.D., 1995, ApJS 99, 427

Taylor C., Thomas D., Brinks E., Skilmann E.D., 1996, ApJS 107, 143

Telles E., Terlevich R., 1995, MNRAS 275, 1

Toomre A., 1970, In: Becker W., Contopoulos G. (eds.) IAU Symp. 38, The Spiral Structure of Our Galaxy. Dordrecht, Reidel, 109

Toomre A., Toomre J., 1972, ApJ 178, 623

Vacca W.D., Conti P.S., 1992, ApJ 401, 543

Vílchez J.M., Esteban C., 1996, MNRAS 280, 720

Vorontsov-Vel'yaminov B.A., 1962, Catalogue of Galaxies and Clusters of Galaxies VII (Moscow:Izd. MGU)

Vorontsov-Vel'yaminov B.A., Arkhipova V.P., 1964, Morphological Catalog of Galaxies Vol. 2 (Moscow:Izd. MGU)

Vorontsov-Vel'yaminov B.A., Dostal' V.A., Metlov V.G., 1981, Sov. Astron. Lett. 6, 217

Walter F., Brinks E., Duric N., Klein U., 1997, AJ 113, 2031

Whitford A.E., 1958, AJ 63, 201

Zaritsky D., Kennicutt R.C. Jr., Huchra J.P., 1994, ApJ 420, 87

Zwicky F., 1968, Catalogue of Galaxies and of Clusters of Galaxies. California Institute of Technology, Pasadena